Eur Biophys J (1994) 23:59–70

European Biophysics Journal

Structures and molecular dynamics of plant waxes

II. Cuticular waxes from leaves of *Fagus sylvatica* L. and *Hordeum vulgare* L.

E. C. Reynhardt [1], **M. Riederer** [2]

[1] Department of Physics, University of South Africa, P.O. Box 392, Pretoria 0001, South Africa
[2] Physiologische Ökologie, Universität Kaiserslautern, Postfach 30 49, D-67618 Kaiserslautern, Germany

Received: 1 June 1993 / Accepted in revised form: 14 October 1993

Abstract. Waxes from the leaves of *Fagus sylvatica* L. (European beech tree) and *Hordeum vulgare* L. (barley) have been investigated using NMR, DSC, X-ray diffraction and gas chromatographic methods. The wax from *Fagus sylvatica*, consisting mainly of *n*-alkanals, *n*-alkanes and 1-alkanols, has chain-lengths ranging from 20 to 52 carbon atoms with an average chain-length of 30.5 carbon atoms. The X-ray results show that the wax is to a large extent (~70%) amorphous. The wax from the leaves of *Hordeum vulgare* L., consisting mainly of *n*-alkanols, has chain-lengths ranging from 20 to 50 carbon atoms with an average chain-length of 27.4 carbon atoms. The wax is ~52% crystalline. It seems that the structure of this wax differs from those of other plant waxes that have been investigated in that the longer chains bridge the amorphous zone between two adjacent layers of crystalline material, thus linking the two layers. This linking affects the melting point of the wax noticeably. The activation energies for the different molecular motions in these waxes have been extracted from the NMR spin-lattice relaxation time measurement.

Key words: Cuticular wax – Chain-length distribution – Molecular motions – Crystallinity – Phase transitions

1. Introduction

The plant cuticle is a very thin skin that covers the leaves, fruits, stems and flowers of higher plants and serves as a protective barrier to the environment, controlling excessive water and nutrient losses. The matrix of this extracellular lipophilic membrane consists of the biopolymer cutin which is essentially an amorphous polyester of hydroxyalkanoic acids (Kolattukudy 1980; Holloway 1982). Cuticular waxes embedded within this matrix and deposited ont its outer surface, consist of a mixture of long-chain aliphatic components (Baker 1982).

These waxes represent the main barrier to the diffusive transport of water and solutes across the plant cuticle. Permeabilities increased by two to four orders of magnitude when the waxes were removed by organic solvents (Schönherr 1982; Schönherr and Riederer 1989). There have been numerous attempts to correlate the transport properties of plant cuticles with the chemical composition of their waxes. Recently Riederer and Schneider (1990) suggested that crystalline arrangements of the aliphatic chains of the wax molecules may form the transport limiting barrier of the cuticle. Thus the physical structure of the wax should be a more important determinant of transport across the cuticle than the chemical composition thereof. Consequently it was recognised that the phenomenological description of the transport properties of plant cuticles should be supplemented by the quantitative analysis of the cuticular waxes and the investigation of the physical principles determining these properties.

The composition of the cuticular wax of leaves of *Citrus aurantium L.* (Riederer and Schneider 1990) and various physical properties of plant cuticles such as degree of order and orientation of intracuticular wax deposits, thermal properties of the cuticular matrix membrane and waxes (Kreger 1958; Sitte and Rennier 1963; Eckl and Gruler 1980; Schreiber and Schönherr 1990), have been investigated. More recently cuticles and wax from the leaves of *Citrus aurantium* L. were investigated by Reynhardt and Riederer (1991) using NMR, DSC, X-ray diffraction and gas chromatografic methods. This paper and the present one are Parts I and II, respectively, of a series of papers on the structures and molecular dynamics of plant waxes. Citrus wax, consisting mainly of 1-alkanols and n-alkyl esters, has chain-lengths ranging from 25 to 53 carbon atoms with an average chain-length of 34 carbon atoms. The wax is to a large extent (~80%) amorphous and the crystalline fraction seems to consist

Correspondence to: E. C. Reynhardt

mainly of the n-alkyl esters with an average chain-length of 43.5 carbon atoms. The activation energies for the different molecular motions in the wax were extracted from the NMR spin-lattice relaxation time measurements. It was concluded that the presence of wax molecules does not influence the molecular dynamics of the matrix membranes noticeably.

In this paper the composition, structures and molecular dynamics of cuticular waxes extracted from leaves of the European beech tree (*Fagus sylvatica* L.) and barley (*Hordeum vulgare* L.) are investigated.

2. Experimental details

2.1. Sample preparation

Leaves were harvested on 1989/05/20 from a 60 to 80 year old *Fagus sylvatica* L. tree at Schachtenau at an elevation of about 800 m above sea level in the Bayerischer Wald National Park, E. Bavaria, Germany. At that time (24 days after budbreak) the leaves had attained their final size.

Plants of *Hordeum vulgare* L. (cultivar Andrea) were cultivated in growth chambers under controlled conditions. Fully developed leaves were harvested when the plants had more than three leaves unfolded but did not yet start tillering.

Cuticular waxes were extracted from whole leaves as described previously (Riederer and Schneider 1990) by immersing the leaf blades in chloroform (>99%) for 30 min at 303 K. Average extraction efficiencies were about 90% of the total wax present in fresh leaves.

Samples used in NMR experiments were sealed off in glass ampoules after having been evacuated for several hours.

The mass of the DSC, X-ray diffraction and NMR samples was ~3 mg, ~100 mg and ~30 mg, respectively.

2.2. Analysis of cuticular wax components

For the qualitative determination of the cuticular wax components the wax extracts were separated into compound classes by thin layer chromatography (TLC) on precoated Kieselgel 60 plates with cellulose acetate concentrating zones. TLC was performed under unsaturated sandwich conditions without control of temperature and relative humidity in the chamber. Separation was achieved by consecutive developments with cyclohexane and 1,1,1-trichloroethane.

The components of the waxes were indentified by capillary gas chromatography-mass spectrometry, performed under chromatography conditions as described below, with the exception that helium was used as carrier gas instead of hydrogen. A Hewlett-Packard Series II gas chromatograph with a 5971A mass selective detector was used. Mass spectra were taken in the electron impact mode and identified by comparison with published spectra or with spectra obtained from reference substances.

For qualitative analyses the cuticular waxes extracted from leaves were used without prior separation by liquid chromatographic methods. For derivatisation the solvent of the wax solutions was evaporated in a gentle stream of nitrogen gas and the samples treated with O-(2,3,4,5,6-pentafluorobenzyl)-hydroxylamine in a solution of dry pyridine and methanol (7:3 v/v) for 3 hours at 333 K. After cooling to room temperature, 10 µl of 2,2-dimethoxypropane was added and the samples were heated again for 2 min at 333 K. After cooling the solvent was evaporated in a stream of nitrogen gas and the samples treated with N,N-*bis*-trimethylsilyltrifluoroacetamide in dry pyridine for 30 min at 343 K. Before injection the reaction mixture was diluted as appropriate with chloroform.

Temperature programmed capillary gas chromatography was carried out on a gas chromatograph equipped with a flame ionization detector on an on-column injector. Fused silica WCOT columns (25 mm × 0.32 mm inner diameter covered with 0.13 µm CP-Sil 5 CB) were used. The temperature program was as follows: injection at 323 K, 2 min at 323 K, 40 K min^{-1} up to 473 K, 2 min at 473 K, 3 K min^{-1} up to 573 K, 40 min at 573 K, 3 K min^{-1} up to 593 K. The inlet pressure of the hydrogen carrier gas was adjusted to 40 kPa at the beginning of each run and raised to 150 kPa 42 min after the injection. Where appropriate peak areas were corrected for differential response.

2.3. DSC

DSC thermograms of the waxes and a number of *n*-alkanes, *n*-hexacosane (*n*-C_{26}), *n*-octacosane (*n*-C_{28}) and *n*-tetratetracontane (*n*-C_{44}), were obtained using a Stanton Redcroft 700 instrument. With a view to eliminating possible effects of moisture on the thermograms, they were obtained in a dry nitrogen atmosphere. Heating rates were 10 K min^{-1}.

2.4. Powder X-ray diffraction

The diffraction patterns for the waxes and *n*-C_{28} were obtained at room temperature with Cu Kα radiation. A Seifert MZIV diffractometer with a proportional counter was used. 2θ was varied at a rate of 0.25° min^{-1}.

2.5. NMR

The proton spin-lattice relaxation times in the laboratory frame, T_1, were measured at 200 MHz on a Bruker CXP200 pulse spectrometer by applying a train of sixteen close-spaced 90° pulses, followed at a variable interval τ by a single 90° measuring pulse. Proton T_1 values were obtained from the slopes of semi-log plots of $(M-M_\infty)/M_\infty$ versus τ, where M_∞ is the equilibrium signal intensity and M the signal intensity a time τ after the saturating pulse sequence.

Proton spin-lattice relaxation time measurements in the rotating frame, $T_{1\varrho}$, were also made on the Bruker

CXP200 NMR spectrometer at a rotating field strength of 20 G. A 90° pulse was applied, followed immediately by a field pulse of width τ, phase shifted by 90° with respect to the first pulse. The magnetization, M, was measured immediately after the second pulse as a function of the length of the pulse. The rotating field strength is proportional to the amplitude of the second pulse. $T_{1\varrho}$ values were obtained from the slopes of semi-log plots of M versus τ.

The liquid content of the wax samples, which will be defined in Sect. 4.1, was determined as a function of temperature by using a single 90° pulse and measuring the amplitude of the proton decay signal 300 μs after the pulse, i.e. when the signal is expected to be entirely due to the liquid component of the wax. At each temperature the average of 20 signals was obtained with a repetition rate of 20 s. The measured amplitudes were converted to percentage liquid by assuming that above the melting point of the wax, the sample is completely in the liquid state and that the signal amplitude is proportional to the liquid content after a correction for the effect of the change of the Boltzmann factor on the signal with changing temperature, had been made.

3. Results

3.1. Gas chromatography

The chemical composition of the *Fagus* wax is dominated by the presence of homologous series of long-chain aliphatic compounds (Table 1). The constituents are *n*-alkanals (18.6%), *n*-alkanes (17.9%) and *n*-alkanols (23.2%), esters ($C_{40}-C_{52}$) (20.6%) and *n*-alkanoic acids (19.7%).

The chain-length distribution has two clearly distinct regions (Fig. 1 a). The majority of the wax constituents (~79%) have chain-lengths from C_{20} to C_{30} with a maximum at C_{28}. The remaining 21% of the wax is made up exclusively of *n*-alkyl esters in the range from C_{40} to C_{50} with a maximum at C_{42}.

The chemical composition of the *Hordeum* wax is also dominated by the presence of homologous series of long-chain aliphatic compounds (Table 1). The constituents are *n*-alkanols (87.1%), *n*-alkanes (0.9%), *n*-alkanals (0.5%), *n*-alkyl esters (10.1%) and *n*-alkanoic acids (1.4%).

The chain-length distribution of this wax also has two clearly distinct regions (Fig. 1 b). The majority of the wax constituents (~90%) have chain-lengths from C_{20} to C_{34} with a maximum at C_{26}. The remaining 10% of the wax is made up exclusively of *n*-alkyl esters in the range from C_{39} to C_{50} with a maximum at C_{46}.

Table 1. Relative composition of the cuticular waxes from fully grown leaves of *Fagus sylvatica* L. and *Hordeum vulgare* L.

Compound	Percentage of mass	
	Fagus	*Hordeum*
n-Alkanals		
C_{24}	0.5	
C_{26}	2.9	0.4
C_{28}	15.2	0.1
Total	18.6	0.5
n-Alkanes		
C_{25}	0.8	
C_{26}	0.3	
C_{27}	15.6	
C_{28}	0.6	
C_{29}	0.6	
C_{31}		0.2
C_{33}		0.7
Total	17.9	0.9
n-Alkyl esters		
C_{39}		0.2
C_{40}	3.9	0.2
C_{41}	0.5	
C_{42}	4.7	0.1
C_{43}	0.5	
C_{44}	3.3	1.8
C_{45}	0.3	
C_{46}	1.9	3.5
C_{47}	0.2	
C_{48}	3.1	3.3
C_{49}	0.6	
C_{50}	1.3	1.0
C_{52}	0.3	
Total	20.6	10.1
n-Alkanoic acids		
C_{20}	0.4	
C_{22}		0.7
C_{23}	1.8	
C_{24}	0.7	
C_{26}	1.9	0.7
C_{27}	0.6	
C_{28}	14.3	
Total	19.7	1.4
n-Alkanols		
C_{20}	3.7	0.2
C_{22}	3.8	1.7
C_{24}	2.4	2.6
C_{26}	1.7	80.4
C_{27}		0.1
C_{28}	10.7	1.7
C_{30}	0.9	
C_{34}		0.4
Total	23.2	87.1

3.2. DSC

The *Fagus* wax exhibits two unresolved endothermic peaks (Fig. 2 a), one at 346 K and another one at approximately 340 K. The thermogram of *n*-C_{28} also exhibits two unresolved endothermic peaks, but they are much narrower and occur at lower temperatures.

The *Hordeum* wax exhibits two endothermic peaks at 324 K and 349 K, as shown in Fig. 2 b. A third peak is present as a shoulder at ~342 K. The thermogram of *n*-C_{26} exhibits two endothermic peaks, but they are much narrower and occur at lower temperatures. The thermogram for *n*-C_{44} has two endothermic peaks, viz. at 352 K and 363 K.

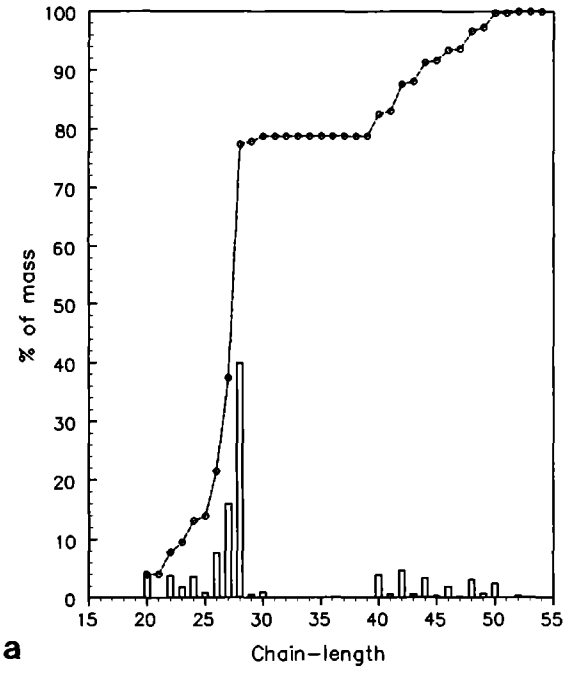

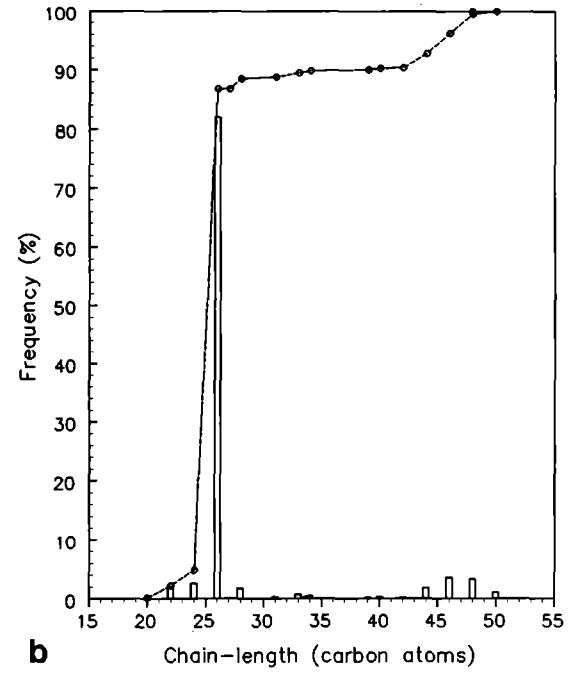

Fig. 1. Individual and cumulative chain-length distributions of the cuticular waxes from leaves of **a** *Fagus sylvatica* L. and **b** *Hordeum vulgare* L.

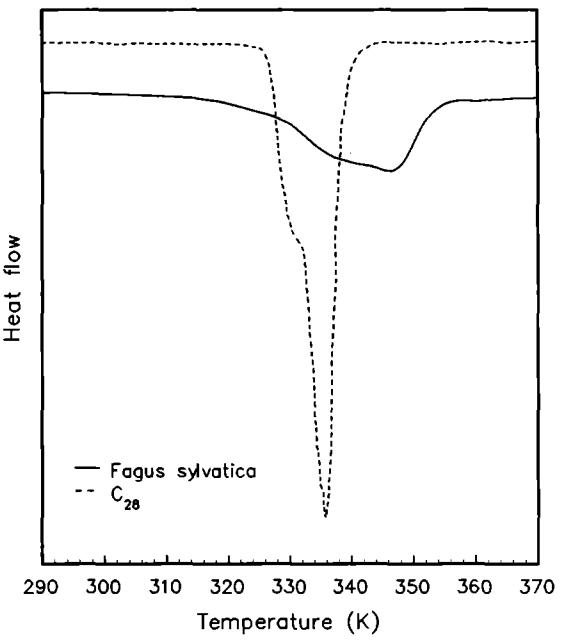

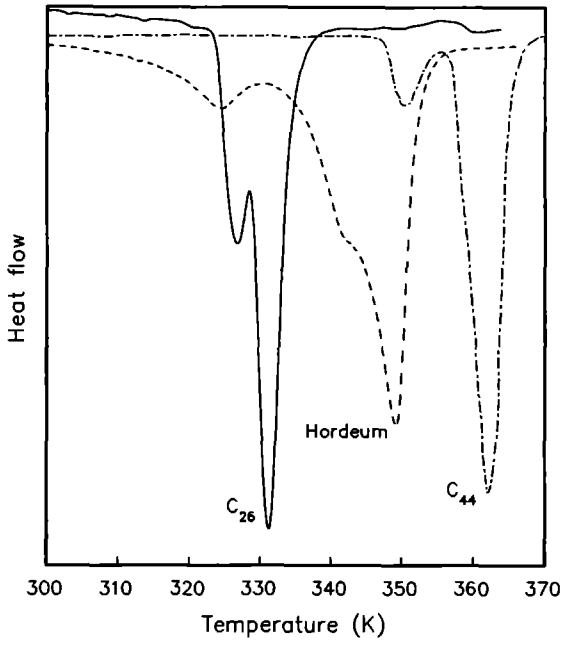

Fig. 2. DSC thermograms for **a** *F. sylvatica* wax and n-C_{28} samples and **b** *Hordeum vulgare* wax, n-C_{26} and n-C_{44} samples

The total enthalphy of all the transitions of the *Hordeum* wax sample is ~46 kJ/kg. Since the sample starts melting at ~265 K, the transitions at 324 K and 342 K are superimposed on the very wide melting transition and, therefore, it was not possible to extract the enthalpies of the overlapping transitions. The total enthalpies for C_{26} and C_{44} are 53 kJ/kg and 122 kJ/kg, respectively.

3.3. X-ray powder diffraction

The X-ray diffractograms of the *Fagus* wax sample is shown in Fig. 3 a. It reveals only two peaks in the range $2° < 2\theta < 30°$. These peaks are superimposed on a very broad peak centered at approximately 20°.

The X-ray diffractograms of the *Hordeum* wax sample is shown in Fig. 3 b. It reveals only two strong peaks in

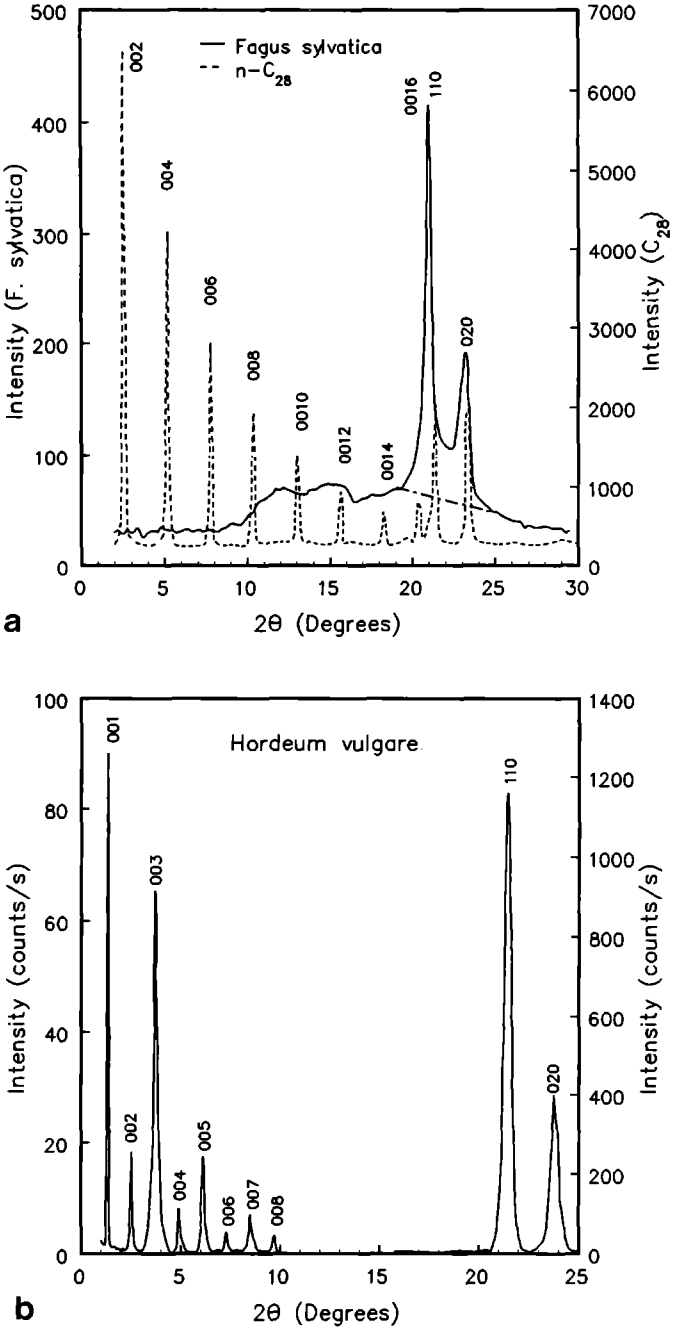

Fig. 3. X-ray powder diffraction spectra of **a** C_{28} and *F. sylvatica* wax and **b** *Hordeum vulgare* wax. In **b** the vertical scales on the left and right refer to the ranges $1° < 2\theta < 15°$ and $15° < 2\theta < 25°$ respectively

the range $1° < 2\theta < 25°$. However, increasing the sampling time by a factor of 20 resulted in a number of weak peaks in the range $1° < 2\theta < 12°$, as shown in the same figure.

3.4. NMR

The liquid content of the *Fagus* wax sample is shown as a function of temperature in Fig. 4a. Below about 285 K it is within experimental error equal to zero, but as the temperature is increased, it increases rapidly to 100% in

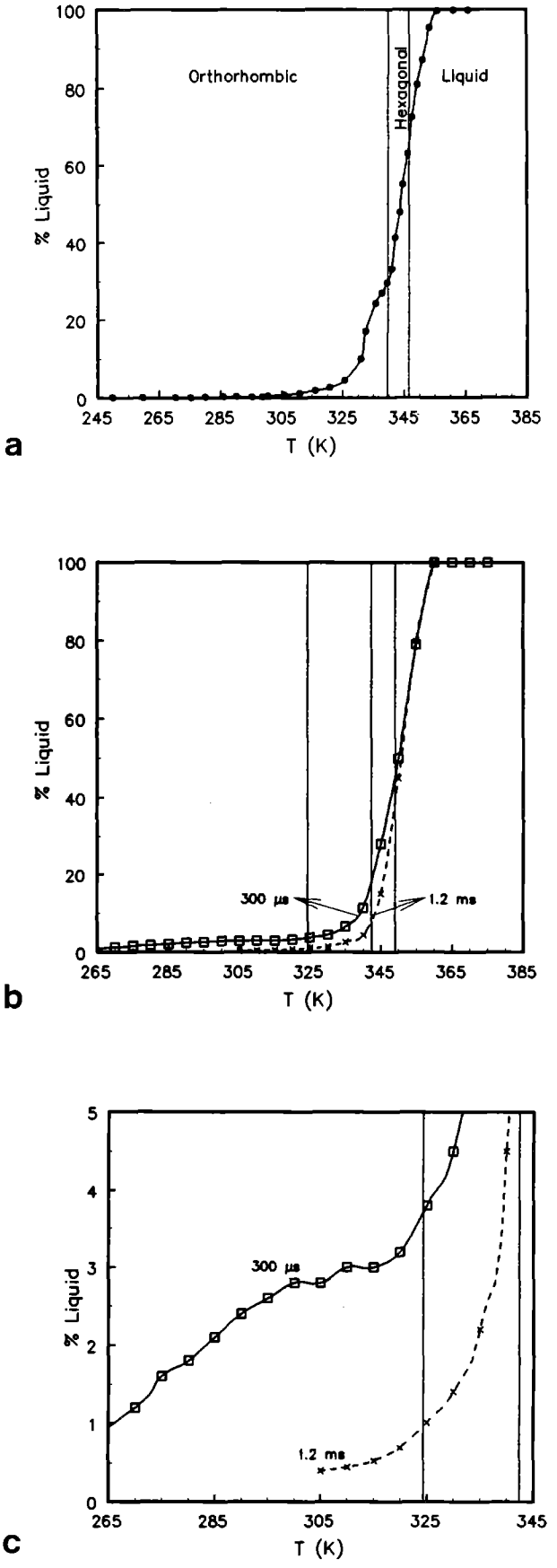

Fig. 4. The liquid content of **a** *F. sylvatica* wax and **b** *H. vulgare* wax as a function of temperature. *Vertical lines* indicate the transition temperatures revealed by the DSC thermogram. In **c** the *lower part* of **b** is magnified

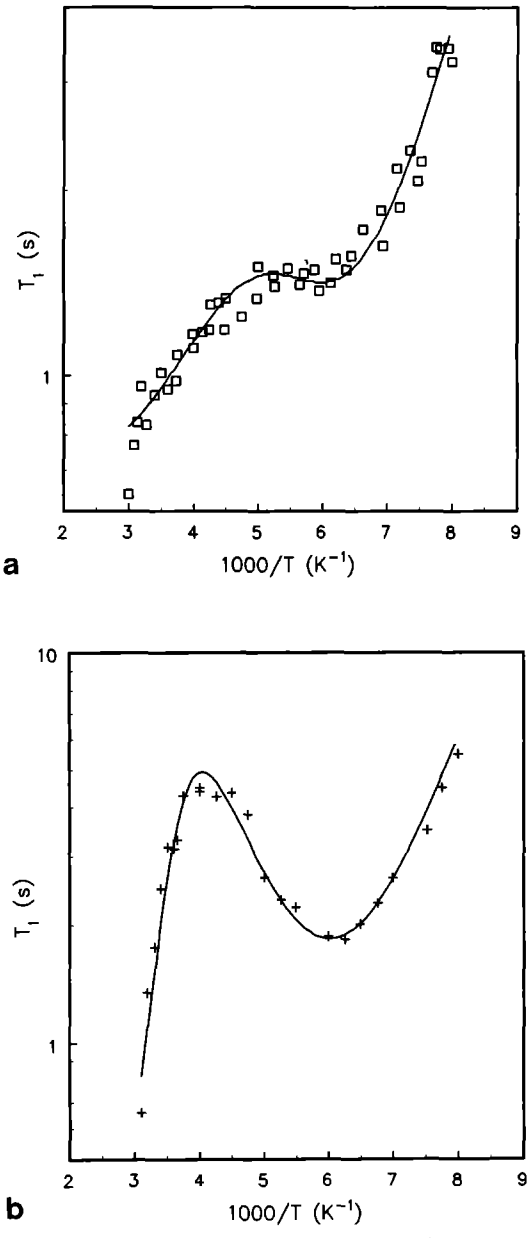

Fig. 5. Proton spin-lattice relaxation time in the laboratory frame as a function of inverse temperature for **a** *F. sylvatica* wax and **b** *H. vulgare* wax. The *solid lines* are fits of Eq. (4) to the data

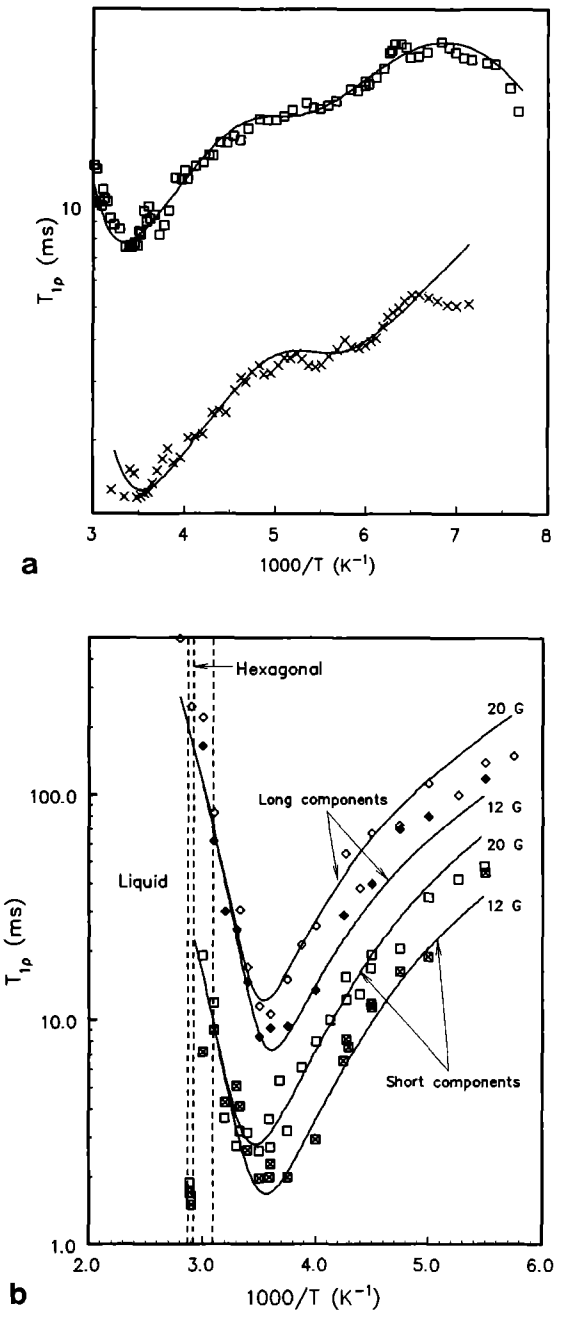

Fig. 6. Proton spin-lattice relaxation times in the rotating frame as a function of inverse temperature for **a** *F. sylvatica* wax and **b** *H. vulgare* wax. The solid lines are fits of Eq. (7) to the data

the vicinity of 355 K. The melting curve shows a discontinuity in the vicinity of the first DSC transition.

T_1 values for this wax are displayed as a function of $1000/T$ in Fig. 5a. These values increase with decreasing temperature, exhibiting an unresolved minimum of approximately 1.5 s at $1000/T \simeq 6\ K^{-1}$.

The magnetization decay curves for the $T_{1\varrho}$ measurements exhibited nonexponential behaviour. Two relaxation components were separated by assuming a relationship of the form

$$M/M_0 = Q\exp(-\tau/T_{1\varrho}^s) + (1-\mathrm{Q})\exp(-\tau/T_{1\varrho}^l), \qquad (1)$$

where M_0 and Q are respectively the magnetization at $\tau = 0$ and the fraction of the protons in the sample relaxing at the faster rate (shorter relaxation time).

The two spin-lattice relaxation times in the rotating frame for the *Fagus* sample are displayed as a function of $1000/T$ in Fig. 6a. The longer relaxation times are about an order of magnitude longer than the shorter ones at corresponding temperatures. The long component exhibits a minimum of ~ 9 ms at $1000/T \simeq 3.4\ K^{-1}$. The temperature dependence of the shorter relaxation time is similar to that of the longer one. A minimum of ~ 1.2 ms occurs at $1000/T \simeq 3.5\ K^{-1}$.

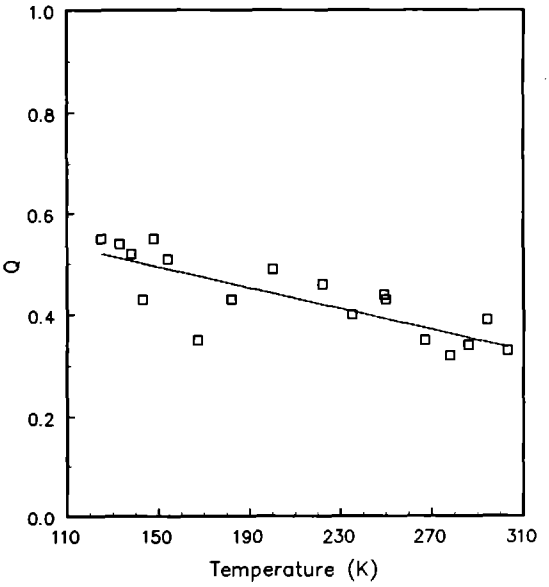

Fig. 7. Temperature dependence of the fraction of protons in the *F. sylvatica* wax sample that relaxes at the faster rate

The values of Q are displayed as a function of temperature in Fig. 7. At room temperature $Q \simeq 0.3$ and it increases slowly with decreasing temperature to ~ 0.5 at 125 K.

The liquid content of the *Hordeum* wax sample is shown as a function of temperature in Fig. 4 b, c for the two measuring positions (300 μs and 1.5 ms). Below about 270 K it is within experimental error equal to zero for the 300 μs position, but as the temperature is increased, it increases slowly to about 5% in the vicinity of 330 K and then rapidly to 100% at 355 K. In the case of the 1.5 ms measuring position, the liquid content is almost zero below ~ 300 K, increases slowly to $\sim 1\%$ at 325 K and rapidly to 100% above this temperature.

T_1 values for this wax are displayed as a function of $1000/T$ in Fig. 5 b. A well-resolved minimum of 1.9 ms occurs at $1000/T \simeq 6\ K^{-1}$. Above 250 K T_1 decreases sharply with increasing temperature without reaching a minimum before the first solid-solid phase transition occurs (324 K).

Two relaxation times in the rotating frame were obtained from the magnetization versus time plots (Fig. 6 b).

4. Discussion

4.1. DSC

The final endothermic peak in Fig. 2 a is associated with the melting of the *Fagus* sample. The other peak is most probably due to the transition to the hexagonal phase, which has been reported for waxes and mixtures of *n*-alkanes (Basson and Reynhardt 1991).

Similarly, the final endothermic peak in Fig. 2 b is associated with the melting of the *Hordeum* wax sample. The shoulder at 342 K is due to the transition to the hexagonal phase. In contrast with other waxes, the wax from leaves of *Hordeum vulgare* shows a second solid-solid transition at ~ 324 K. Strobl et al. (1974) observed two solid-solid transitions prior to the hexagonal transition in n-C_{33} single crystals. These transitions were found to be related to specific types of orientational disorder of the chains. Since single crystals of waxes with wide chain-length distributions have not been grown successfully, it was not possible to investigate the structures of the solid phases of *Hordeum* wax in detail with the equipment at our disposal. However, it is clear that the crystalline zone of *Hordeum* wax differs structurally from those of *Citrus aurantium* L. and *Fagus sylvatica* L.

4.2. Structure

The structure of a wax (Le Roux and Loubser 1980; Basson and Reynhardt 1992 b) is illustrated in Fig. 8. Zone A closely resembles a pure crystalline *n*-alkane. This zone has an orthorhombic structure that transforms into an hexagonal phase just below the temperature at which the wax is fully melted (Reynhardt 1986). Zone B is the solid amorphous zone and contains chain-ends. The size of this zone depends on the width of the chain-length distribution and the population of defect orientations. If the distribution is approximately Gaussian, the root mean square deviation from the mean, σ, gives an indication of the extent of zone B. Zone C is the rigid amorphous zone containing defects caused by branches. In plant waxes this zone is usually relatively small. Mobile amorphous zone D mainly consists of the shortest chains that end up between crystallites during crystallization. However, it is not entirely separated from the rest of the structure since a fraction of it occupies the voids in amorphous zone B. This fraction is determined by the temperature and the width of the total chain-length distribution. It has been shown (Basson and Reynhardt 1992 b) that with increasing temperature the mobile amorphous zone initially forms inside zone B and that it starts forming outside this zone only after the voids in zone B have been filled.

4.2.1. X-ray powder diffraction. All waxes have an orthorhombic crystalline fraction at temperatures below the hexagonal phase transition (Chichakli and Jessen 1967; Ratnasamy et al. 1973; Reynhardt 1986). The *a* and *b* cell dimensions are the same as those for *n*-alkanes, viz. ~ 5.0 and ~ 7.5 Å respectively (Broadhurst 1962).

The X-ray diffractogram of a wax shows diffraction peaks from lattice planes in crystalline zone A only. The amorphous component, consisting of zones B, C and D in Fig. 8, contributes only to a broad peak, characteristic of diffraction from noncrystalline material, ranging from $\sim 8°$ to $\sim 30°$ in Fig. 3 a for *Fagus* wax. The two narrow peaks, superimposed on the broad peak, are the 110 and 020 reflections. Since waxes and *n*-alkanes have very long *c* axes, reflections from 00*l* planes are observed as low angle diffraction peaks. The fact that no such diffraction peaks are observable in Fig. 3 a, suggests that, owing to the wide distribution of chain-lengths, the 00*l* planes are not well-defined in the *Fagus* sample.

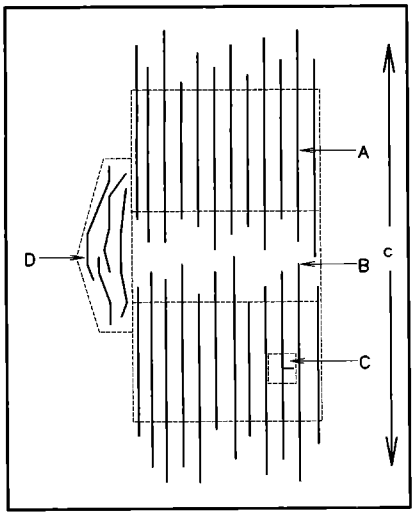

a

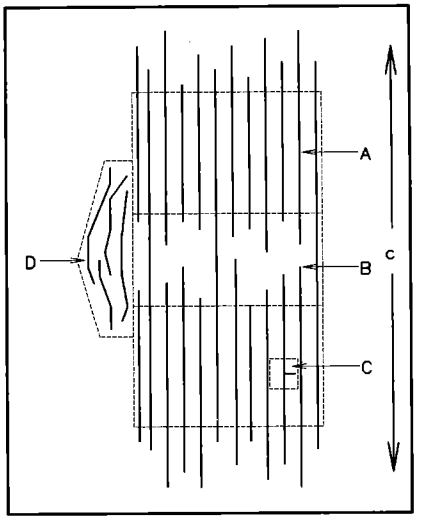

b

Fig. 8. **a** Representation of the structure of a wax with a normal distribution of chain lengths. The different zones are discussed in the text. **b** Model for the structure of wax from leaves of *Hordeum vulgare*, showing the linking of the two crystalline phases by longer chains

Also included in Fig. 3a is the diffractogram of fully crystalline n-C_{28}. Apart from the fact that the 00l peaks are narrow and strong, the 110 and 020 peaks are much stronger than the corresponding peaks in the diffractogram of the *Fagus* wax. Since the samples had the same size and roughly the same composition (long aliphatic chains with average chain-length 28 carbon atoms) and the diffractograms were obtained under identical conditions, it seems that the *Fagus* wax sample has a low crystallinity.

The length of the c axis of the unit cell of the *Hordeum* wax sample can be determined from the weak 00l reflections shown in Fig. 3b. Using

$$c = \lambda l / 2 \sin\theta, \qquad (2)$$

where λ is the wavelength of the X-rays (1.5418 Å), a good fit to the observed peak positions was obtained with $c = 70 \pm 1$ Å and $l = 1$ to 8. The length of the c axis of a mixture of chain-like molecules can also be determined from (Broadhurst 1962; Nyburg and Potworowski 1973)

$$c = 2.54n + 2\delta, \qquad (3)$$

where δ is an end-correction determined by the packing of the chains. Stokhuyzen and Pistorius (1970) determined a value of 2.25 Å for n-alkane mixtures and wax fractions. Substituting this value for δ and $c = 70$ Å into Eq. (2), it follows that $n \simeq 26$ carbon atoms. It seems that the c cell dimensions is determined to a large extent by the C_{26} chains of the wax. Since more than 80% of the chains in the sample are C_{26} chains, this result is not unexpected. However, from the DSC thermograms it is clear that the wax differs structurally considerably from n-C_{26}. It is unlikely that the longer chains ($n > 40$) form a mobile amorphous zone either by occupying voids in the B zone or by forming such a zone outside the B zone. It is more likely that these longer chains are oriented parallel to the shorter chains and that they bridge amorphous zone B, thus linking two crystalline zones, as shown in Fig. 8.

It is anticipated that such a linking of adjacent crystalline zones would play a significant role in the physical properties of the wax. From the thermograms (Fig. 2b) it can be seen that, although the wax consists to a very large extent (80%) of C_{26} chains, the melting point of the wax (349 K) is closer to that of n-C_{44} (362 K) than to that of n-C_{26} (331 K). From studies of n-alkanes and n-alkane mixtures (Basson and Reynhardt 1990, 1992a), it is known that the melting points of mixtures of n-alkanes with the same average chain-length and distribution widths up to $\sigma = 5$ carbon atoms, are approximately the same as that of an n-alkane with chain-length equal to the average chain-length of the mixtures. Therefore, without the long n-alkyl ester chains (10% of the mass of the sample) the melting point of the wax would be approximately 331 K, the melting point of n-C_{26}. It is clear that the linking of adjacent crystalline zones increases the melting point of the wax considerably.

While 00l reflections with l odd are systematically absent for n-alkane mixtures and waxes that have been investigated (Basson and Reynhardt 1991), 1992a; Reynhardt and Riederer 1991), this condition seems to be invalid in the case of *Hordeum vulgare* wax.

4.2.2. Crystallinity. A rough estimate of the crystallinity of the wax samples can be obtained by assuming that the diffractograms of the wax samples, consisting only of zone A, would be the same as that of a dimensionally identical n-C_{28} sample. The total area under the 110 and 020 peaks of a wax sample (A_{wax}) and the area under the corresponding peaks of an n-C_{28} sample (A_{28}) are compared. Since the n-C_{28} sample is fully crystalline, the ratio A_{wax}/A_{28} should give a reliable indication of the crystallinity of the wax sample. With a view to obtaining the area under the 110 and 020 wax peaks, a linear interpolation, which served as a baseline, was made between the measured intensities at 19° and 25° in Fig. 3a, b. The

ratio A_{wax}/A_{28} was found to be (0.31 ± 0.05) and (0.52 ± 0.5) for *Fagus* and *Hordeum*, respectively. It is therefore concluded that the crystallinity (zone A in Fig. 8) of *Fagus* and *Hordeum* waxes are $(31 \pm 5)\%$ and $(52 \pm 5)\%$, respectively.

It is interesting to note that the amplitude of the FID of the NMR signal associated with $T_{1\varrho}^{s}$ values, Q in Eq. (1), is approximately 0.3 in the vicinity of room temperature, as shown in Fig. 7 for *Fagus*. This value is about the same as the crystallinity of the wax. If it is kept in mind that the ratio Q refers to the relative number of protons in two noninteracting spin systems in the wax, it seems probable that the amorphous and crystalline components correspond to these separate spin systems.

4.3. NMR

4.3.1. Liquid content. Basson and Reynhardt (1992b) have shown that the NMR signal (free induction decay) of a wax has three components. The short component corresponds to crystalline zone A and is shorter than 50 μs. The chains in this zone are rigid and start executing chain reorientations only close to the hexagonal phase transition. The second component is shorter than 1 ms and represents the chain-ends in zone B and the chains of the D zone that fill the voids in zone B. These chains have more mobility than those in zone A. The free induction decay of zone D, excluding the fraction occupying voids in zone B, is longer than 1 ms. The chains in this part of zone D have a large degree of motional freedom and resemble a liquid.

Figures 4b and 4c illustrate that *Hordeum vulgare* wax, like other waxes (Reynhardt 1985a, b; Basson and Reynhardt 1988a, b, c; Reynhardt and Riederer 1991), melts over a fairly wide temperature range (~ 100 K). At 265 K the wax is entirely in the solid state, while at 360 K it is completely in the liquid state. Between 265 K and 300 K only the 300 μs measuring position shows a mobile component and, therefore, the mobile amorphous zone D is absent or restricted to the voids in zone B. If zone D is absent, the mobility measured at 300 μs could be due to the defect motions of chain ends. At temperatures above 305 K the mobile amorphous zone starts forming outside zone B, as revealed by the results obtained at the 1.5 ms measuring position. The transition to the hexagonal phase (~ 342 K) roughly coincides with the sharp increase in the liquid content with increasing temperature. It is well-known that the chains are much more mobile in the hexagonal (rotator) phase than in the orthorhombic phase.

At 285 K the *Fagus* wax is entirely in the solid state, while at 355 K it is completely in the liquid state (Fig. 4a). It is interesting that the transition to the hexagonal phase (~ 340 K) coincides with a discontinuity in the graph of liquid content versus temperature.

No information has been obtained concerning the chemical identity of amorphous zone D of these plant waxes. However, it can be assumed that it contains cylic wax constituents which, owing to their structural properties, cannot be accommodated in crystalline zone A. Thus, this zone of the two waxes will contain components such as caffeic acid (3-(3,4-dihydroxyphenyl)-2-propenoic acid), *p*-coumaric acid (3-(4-hydroxyphenyl)-2-propenoic acid), oleanoic acid (3-hydroxyolean-12-en-28-oic acid), hederagenin (3,23-dihydroxyolean-12-en-28-ioc acid) and β-sitosterol (stigmast-5-en-3-ol), which have been identified in the non-aliphatic fraction of *Fagus* leaf wax (Schneider 1990). However, in view of its temperature dependent volume fraction, even at room temperature it is possible that zone D contains some of the long-chain aliphatic wax constituents not incorporated in zone A. The aliphatic chain content of zone D increases with increasing temperature (see Fig. 4) and in the vicinity of 355 K almost all the aliphatic chains form part of zone D.

4.3.2. Model for the melting of the wax. A simple model for the melting of a wax, based on the results of the present and other investigations (Le Roux and Loubser 1980; Reynhardt 1985a, b, 1986; Basson and Reynhardt 1992b), will now be described.

Just below the transition to the hexagonal phase, the structure of the wax corresponds to the one illustrated in Fig. 8a. However, mobile amorphous zone D, consisting of the shorter chains of the wax, is not entirely separated from the rest of the structure, but also occupies the voids in amorphous zone B. The length of the longest chains in this zone is determined by the temperature and the width of the total chain-length distribution. The chain-ends of longer chains belonging to crystalline zone A excecute fast *trans-gauche* defect motions, while the shorter chains in this zone are involved in rapid translational-rotational motions (Sect. 4.3.3) (Basson and Reynhardt 1991, 1992a). A decrease in temperature results in the partial solidification of mobile amorphous zone D. Some of the longest chains become part of the crystalline zone, while others start forming a solid amorphous zone. At lower temperatures the transformation of the mobile amorphous zone into the solid amorphous zone (also D in Fig. 8) is complete and the occupation of defect orientations of chain-ends in amorphous zone B is decreased, while the translational-reorientational motions of the shorter chains in crystalline zone A are slowed down. At still lower temperatures only threefold reorientations of methyl groups (Sect. 4.3.2) are present.

If the sample is now heated to the hexagonal transition, chain-end defect reorientations and translational-reorientational motions in amorphous and crystalline regions B and A respectively become activated. The shortest chains in the solid amorphous zone become mobile and mobile amorphous zone D appears. Just below the phase transition this process is complete, i.e. the solid amorphous zone has been converted totally into the mobile amorphous zone.

In the hexagonal phase the chains are rotating about their long axes, while the defect motions of chain-ends are highly populated (Maroncelli et al. 1985a, b). The Van der Waals forces between molecules are weakened and the shorter chains leave the crystalline zone to become part of the mobile amorphous zone. The melting process is complete when the entire sample is in the mobile amorphous zone.

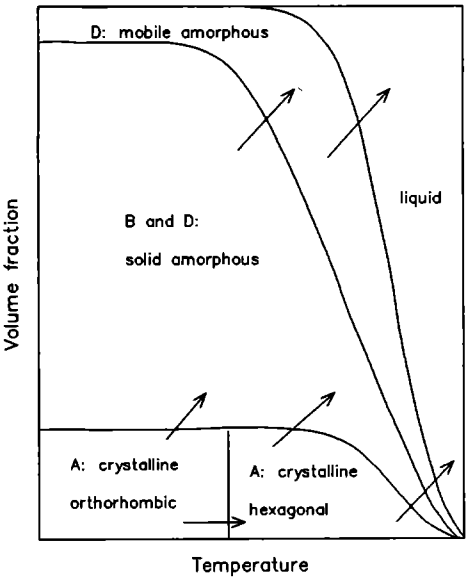

Fig. 9. Diagrammatical representation of the melting of different zones of a wax as a function of temperature

As illustrated in Fig. 9, the melting process takes place in two stages. The first stage is the melting of the solid amorphous zone and the second stage the melting of the crystalline zone and therefore also the amorphous zone.

4.3.3. Spin-lattice relaxation times in the laboratory frame. The T_1 minumum observed for each of the wax samples is associated with threefold reorientations of methyl groups. The relaxation rate due to these reorientations is given by (Kubo and Tomita 1954)

$$1/T_1 = 2/3\,\gamma^2 h^2\,\Delta M_2 \times \{\tau_c/(1+\omega_0^2\,\tau_c^2) + 4\,\tau_c/(1+4\,\omega_0^2\,\tau_c^2)\} \quad (4)$$

where

$$\tau_c = \tau_0 \exp(E/RT), \quad (5)$$

ω_0 is the Larmor frequency, γ the gyromagnetic ratio for protons and ΔM_2 the proton second moment reduction due to the methyl reorientations.

It is clear that at least two motions are required for each wax to obtain a fit of Eq. (4) to the experimental T_1 results shown in Fig. 5. Since a minimum was not reached in the high temperature region, all the information on the motional mechanisms which dominate the relaxation rate in the high temperature region could not be obtained from the T_1 results. However, in Sect. 4.5.3 these motions will be discussed in detail. The best fit of Eq. (4) to the experimental data yields $E = 8.4 \pm 0.8$ kJ/mol, $\tau_0 = (7 \pm 2) \times 10^{-13}$ s and $\Delta M_2 = 1.0 \pm 0.1$ G^2 for *Fagus* wax and $E = 8.4 \pm 0.8$ kJ/mol, $\tau_0 = (1.2 \pm 0.5) \times 10^{-12}$ s and $\Delta M_2 = 1.0 \pm 0.1$ G^2 for *Hordeum* wax. The activation energies for the high temperature mechanisms are ~8 kJ/mol and ~30 kJ/mol, respectively, but it will be shown that because of the overlapping of two mechanisms, these values are misleading.

A calculation based on the information listed in Table 1 revealed that 6.2% of all protons in the *Fagus* sample belong to methyl groups. The second moment reduction associated with an isolated reorienting methyl group is 16.9 G^2 and therefore the expected second moment reduction for the simultaneous reorientation of all methyl groups in the sample is (0.062×16.9 $G^2 =$) 1.0 G^2. This value is in excellent agreement with the experimentally obtained value of 1.0 ± 0.1 G^2. It is therefore concluded that all methyl groups in the sample execute threefold reorientations with approximately the same motional parameters.

Similarly, 5.4% of all protons in the *Hordeum* sample belong to methyl groups and the expected second moment reduction for the simultaneous reorientation of all methyl groups in the sample is (0.054×16.9 $G^2 =$) 0.91 G^2. Since this value is in excellent agreement with the experimentally obtained value of 1.0 ± 0.1 G^2, it is concluded that all methyl groups in this sample also execute threefold reorientations with approximately the same motional parameters.

4.3.4. Spin-lattice relaxation time in the rotating frame. It was not possible to fit the single correlation time model (Bloembergen et al. 1948) to the $T_{1\varrho}$ data for the wax samples. However, good fits, shown as solid lines in Fig. 6, were obtained by substituting the Davidson-Cole spectral density function (Davidson and Cole 1951)

$$J(\omega, \varepsilon) = 2/\omega \{\sin[\varepsilon \arctan(\omega\tau)]/(1+\omega^2\,\tau^2)^{\varepsilon/2}\} \quad (6)$$

into the general expression (Abragam 1961)

$$1/T_{1\varrho} = \gamma^2 \mathrm{h}^2\,\Delta M_2 \times \{J(2\omega_1, \varepsilon) + 5/3\,J(\omega_0, \varepsilon) + 2/3\,J(2\omega_0, \varepsilon)\} \quad (7)$$

and varying the parameters E, τ_0, ε and ΔM_2. The parameter ε specifies the width of the distribution of correlation times and is limited to the range $0 < \varepsilon \leqq 1$. If $\varepsilon = 1$, Eq. (7) reduces to the BPP spectral density function (Bloembergen et al. 1948). The values of the fitting parameters thus obtained are listed in Tables 2 and 3 for *Fagus and Hordeum*, respectively.

Nonexponential decay of the magnetization in the rotating frame was also observed in the case of *Citrus aurantium* L. (Reynhardt and Riederer 1991) and ascribed to the crystalline and amorphous components of the wax forming two noninteracting spin systems. The shorter relaxation time were associated with the crystalline component of the wax. In this paper it will be assumed that the nonexponential relaxation is also due to the crystalline and amorphous components of the wax and that the shorter relaxation time is associated with the former component. The fact that the shorter relaxation time shows a sudden decrease of an order of magnitude at the transition to the hexagonal phase, while the longer relaxation time shows no discontinuity at that temperature, supports the abovementioned interpretation of the nonexponentiality.

The temperature dependence of the values of $T_{1\varrho}^s$ and $T_{1\varrho}^l$ (Fig. 6) resembles that of binary and multiple mixtures of *n*-alkanes (Basson and Reynhardt 1991, 1992a). In these mixtures two motions were isolated in the high temperature region. The first motion, resulting in an unresolved $T_{1\varrho}$ minimum in the vicinity of $1000/T = 5.5\,\mathrm{K}^{-1}$, is the defect motion of chain-ends of longer

Table 2. Motional parameters for chains in *F. sylvatica* wax

Motion	E (kJ/mol)	$\log\{\tau_0(s)\}$	ε	$\Delta M_2(G^2)$
Methyl threefold	8.4±0.8	−(12.2±0.2)		1.0±0.1
Solid amorphous zone:				
Long chains defect	19±2	−(11.0±0.2)	0.3±0.1	0.2±0.02
Short chains twofold screw	38±5	−(12.0±0.2)	0.2±0.1	0.9±0.3
Crystalline and amorphous zones:				
Long chains defect	19±2	−(11.4±0.2)	0.3±0.1	1.0±0.1
Short chains twofold screw	36±5	−(12.0±0.2)	0.2±0.1	5.0±1.0

Table 3. Motional parameters for chains in *Hordeum vulgare* wax

Motion	E (kJ/mol)	$\log\{\tau_0(s)\}$	ε	$\Delta M_2(G^2)$
Methyl threefold	8.4±0.8	−(11.9±0.2)		1.0±0.1
Zone D:				
Long chains defect	33±2	−(11.7±0.2)	0.2±0.1	0.2±0.02
Short chains twofold screw	67±9	−(18.0±0.5)	0.4±0.2	0.3±0.1
Zones A and B:				
Long chains defect	33±2	−(11.7±0.5)	0.2±0.1	0.4±0.1
Short chains twofold screw	50±8	−(14.8±0.5)	0.5±0.2	1.3±1.0

chains. The defect orientations are less populated than the normal all-trans orientation, but as the temperature is increased, the population of the defect orientations increases. However, if the distribution width of the mixture is too wide ($\Delta N > 3$ carbon atoms), folding of the chains occurs which hampers the defect motions. $T_{1\varrho}$ minima at $1000/T \simeq 3.4\ K^{-1}$ are associated with twofold screw motions (translational-reorientational) of the shorter chains. If the defect orientations of the longer chains are highly populated, the motions of the shorter chains are hampered. In these cases it was not possible to obtain realistic fits to the relaxation data using one of the standard correlation distribution function (Beckmann 1988). However, a model based on a stretched exponential distribution function (Williams and Watts 1970; Ngai 1979), yielded good fits to the data.

At this stage it should be emphasized that the molecular dynamics of two separate chain-length distributions, like the ones which have so far been encountered in cuticular waxes, have not been studied extensively. Experiments in which the molecular dynamics of two separate samples of *n*-alkane mixtures, representing the two distributions, and a mixture of these two samples are studied, should shed more light on this aspect. Such experiments are being executed.

However, on account of the models for molecular motions in mixtures of *n*-alkanes (Basson and Reynhardt 1991, 1992a), it is assumed that the shallow unresolved $T^s_{1\varrho}$ minimum associated with the crystalline component reflects the defect motions of chain-ends of the longer chains, while the deeper minimum is due to the twofold screw motions of the shorter chains.

The longer values, $T^l_{1\varrho}$, are associated with the solid amorphous zone of the waxes. Apart from its amorphousness, the main difference between it an the rest of the sample is that its average chain-length is much shorter than that of the rest of the sample. Since defect orientations of chain-ends in short chains ($n < 24$) have very low populations in the orthorhombic phase (Maroncelli et al. 1985a, b; Basson and Reynhardt 1990, 1991), the spin-lattice relaxation time associated with this mechanism is expected to be longer in the solid amorphous zone compared to the corresponding value at the same temperature in the rest of the sample. It is also reasonable to assume that the translational-reorientational motions will be severely restricted in an amorphous mixture of chains, resulting in a shallower $T^l_{1\varrho}$ minimum at higher temperatures, as was observed experimentally.

4.4. Biological relevance

This study has established a structural model for the cuticular transport barrier, proposed earlier by Riederer and Schneider (1990). The low permeability of this barrier to water and solutes (Schönherr 1982; Schönherr and Riederer 1989) can be explained in terms of the crystalline wax domains within the cuticle. Molecules diffusing across the transport barrier are excluded from the crystalline domains, thus reducing the cross-sectional area available for diffusion and increasing the effective path length.

Diffuse transport of water or solutes is restricted to the amorphous fraction of the wax. Owing to the absence of a discrete structural order, this zone is accessible to permeating molecules, which can easily diffuse in this material of relatively high fluidity. How the chemical composition of the wax (especially the fractions of short chains and non-aliphatic constituents) affects the extent of amorphous zone D an whether it leads to changes in cuticular permeability, will have to be addressed by further studies. Since elevated temperatures lead to an increase of zone D in waxes, the concomitant effect on cuticular permeability should also be studied.

The crystallinity of the three plant waxes which have been investigated so far is 20% (*Citrus aurantium* L.), 30% (*Fagus sylvatica* L.) and 52% (*Hordeum vulgare* L.). This wide range of experimentally determined crystallinities offers the opportunity to test the validity of the proposed model for the cuticular transport barrier.

The linking of adjacent crystalline zones within a crystallite by longer chains seems to be a very effective way of

increasing the transition temperatures, including the melting point, of a wax. Since it is possible that a higher melting point may be obtained without considerably increasing the hardness of a wax, and therefore its pliability, it is possible that the compostion of plant waxes could be of interest to the synthetic wax industry.

Acknowledgements. This work was supported in part by a grant from the Deutsche Forschungsgemeinschaft. Financial support from the Research and Bursaries Committee of the University of South Africa and the Foundation for Research Development is also acknowledged. The authors are indebted to R. Jetter for his assistance in the qualitative analysis of the *Hordeum* wax and the Nationalparkverwaltung Bayerischer Wald, Grafenau, for technical support and permission to take the leaf samples in the national park area.

References

Abragam A (1961) The principles of nuclear magnetism. Oxford University Press, London, pp 289–305

Baker EA (1982) Chemistry and morphology of plant epicuticular waxes. In: Cutler DF, Alvin KL, Price CE (eds) The plant cuticle. Academic Press, London, pp 139–165

Basson I, Reynhardt EC (1988a) An investigation of the structures and molecular dynamics of natural waxes: I. Beeswax. J Phys D: Appl Phys 21:1421–1428

Basson I, Reynhardt EC (1988b) An investigation of the structures and molecular dynamics of natural waxes: II. Carnauba wax. J Phys D: Appl Phys 21:1429–1433

Basson I, Reynhardt EC (1988c) An investigation of the structures and molecular dynamics of natural waxes: III. Montan wax. J Phys D: Appl Phys 21:1434–1437

Basson I, Reynhardt EC (1990) Identification of a defect chain motions in n-alkanes by means of nuclear magnetic resonance spin-lattice relaxation time measurements. J Chem Phys 93:3604–3609

Basson I, Reynhardt EC (1991) Identification of defect chain motions in the low temperature orthorhombic phase of binary mixtures of n-alkanes by means of nuclear magnetic resonance spin-lattice relaxation time measurements. J Chem Phys 95:1215–1222

Basson I, Reynhardt EC (1992a) Defect chain motions in the low temperature phase of multiple mixtures of n-alkanes by means of nuclear magnetic resonance spin-lattice relaxation time measurements. J Chem Phys 97:1287–1295

Basson I, Reynhardt EC (1992b) The structure and melting of paraffinic Fischer-Tropsch waxes. Chem Phys Lett 198:367–372

Beckmann PA (1988) Spectral densities and nuclear spin relaxation in solids. Phys Rep 171:87–128

Bloembergen N, Purcell EM, Pound RV (1948) Relaxation effects in nuclear magnetic resonance absorption. Phys Rev 73:679–712

Broadhurst MG (1962) An analysis of the solid phase behaviour of the normal paraffins. J Res Nat Bur Stand 66A:241–249

Chichakli M, Jessen FW (1967) Crystal morphology in hydrocarbon systems. Indust and Eng Chem 59:86–98

Davidson DW, Cole RH (1951) Dielectric relaxation in glycerol, propylene glycol and n-propanol. J Chem Phys 19:1484–1490

Eckl K, Gruler H (1980) Phase transitions in plant cuticles. Planta 150:102–113

Holloway PJ (1982) Structure and histochemistry of plant cuticular membranes. In: Cutler DF, Alvin KL, Price CE (eds) The plant cuticle. Academic Press, London, pp 45–85

Kolattukudy PE (1980) Bio-polyester membranes of plants – cutin and suberin source. Science 208:990–1000

Kreger DR (1958) Wax. In: Peach K, Schwarze P (eds) Handbuch der Pflanzenphysiologie, vol 10. Springer, Berlin, pp 249–269

Kubo R, Tomita K (1954) A general theory of magnetic resonance absorption. J Phys Soc J 9:888–919

Le Roux JH, Loubser NH (1980) Nuclear magnetic resonance investigation of the mobile phase in paraffinic Fischer-Tropsch waxes. SA J Sci 76:157–161

Maroncelli M, Strauss HL, Snyder RG (1985a) The distribution of conformational disorder in the high-temperature phases of the crystalline n-alkanes. J Chem Phys 82:2811–2424

Maroncelli M, Strauss HL, Snyder RG (1985b) Structure of the n-alkane binary solid n-$C_{19}H_{40}$/n-$C_{21}H_{44}$ by infrared spectroscopy and calorimetry. J Phys Chem 89:560–5267

Ngai KL (1979) Universality of low-frequency fluctuation, dissipation and relaxation properties of condensed matter. Commun Solid State Phys 9:127–140

Nyburg SC, Potworowski JA (1973) Prediction of unit cells and atomic coordinates for the n-alkanes. Acta Crystallogr B29:347–352

Ratnasamy P, Anand KS, Gupta DC (1973) Structure and properties of microcrystalline waxes. J Appl Chem Biotechnol 23:183–187

Reynhardt EC (1985a) NMR investigation of Fischer-Tropsch waxes: II. Hard wax. J Phys D: Appl Phys 18:1185–1197

Reynhardt EC (1985b) NMR investigation of Fischer-Tropsch waxes: III. ^{13}C and ^{1}H study of oxidized hard wax. J Phys D: Appl Phys 18:2519–2528

Reynhardt EC (1986) Temperature dependence of the cell parameters of Fischer-Tropsch waxes: hard wax and oxidised hard wax. J Phys D: Appl Phys 19:1925–1938

Reynhardt EC, Riederer M (1991) Structure and molecular dynamics of the cuticular wax from leaves of citrus aurantium L. J Phys D: Appl Phys 24:478–486

Riederer M, Schneider G (1990) The effect of the environment on the permeability and composition of citrus leaf cuticles. 2. Composition of soluble cuticular lipids and correlation with transport-properties. Planta 180:154–165

Schneider G (1990) PhD thesis Technische Universität München

Schönherr J (1982) Resistance of plant surfaces to water loss: transport properties of cutin, suberin and associated lipids. In: Lange OL, Nobel PS, Osmond CB, Ziegler H (eds) Encyclopedia of plant physiology, New series vol 12B: Physiological plant ecology, Part 2. Springer, Berlin, pp 153–179

Schönherr J, Riederer M (1989) Foliar penetration and accumulation of organic chemicals in plant cuticles. Rev Environ Contam Toxicol 108:1–70

Schreiber L, Schönherr J (1990) Phase transitions and thermal-expansion coefficients of plant cuticles – the effect of temperature on structure and function. Planta 182:186–193

Sitte P, Rennier R (1963) Cuticular layers of cell walls. Planta 60:19–40

Stokhuyzen R, Pistorius CWFT (1970) Phase behaviour of Fischer-Tropsch wax fraction under high pressure. J Appl Chem 20:1–6

Strobl G, Ewen B, Fischer EW, Piesczek (1974) Defect structure and molecular motion in the four modifications of n-tritriacontane. 1. Study of the defect structure in the lamellar interfaces using small angle X-ray scattering. J Chem Phys 61:5257–5264

Williams G, Watts DC (1970) Non-symmetrical dielectric relaxation behaviour arising from a simple empirical decay function. Trans Faraday Soc 66:80–85